Competition between N−H and N−D Bond Cleavage in the Photodissociation of NH_2D and ND_2H†

Jonathan P. Reid, Richard A. Loomis,‡,§ and Stephen R. Leone*,||

JILA, National Institute of Standards and Technology and University of Colorado, Department of Chemistry and Biochemistry, University of Colorado, Boulder, Colorado 80309-0440

Received: March 21, 2000; In Final Form: May 5, 2000

The adiabatic dissociation dynamics of $NH_2D(\tilde{A})$ and $ND_2H(\tilde{A})$ have been probed by time-resolved Fourier transform infrared emission spectroscopy. A product-state spectral pattern recognition technique is employed to separate out the emission features arising from the different photofragmentation channels following the simultaneous excitation of mixtures of the four parent molecules NH_3, NH_2D, ND_2H, and ND_3 at 193.3 nm. The rotational energy partitioning about the primary *a*-axis of the fragments $NH_2(\tilde{A},v_2' = 0)$ and $ND_2(\tilde{A},v_2' = 0)$ from $NH_2D(\tilde{A})$ and $ND_2H(\tilde{A})$, respectively, is bimodal. We suggest that the origin of this excitation reflects the competition between two distinct dissociation mechanisms that sample two different geometries during the bond cleavage. A larger quantum yield for producing $ND_2(\tilde{A},v_2' = 0)$ from the photodissociation of ND_2H than ND_3 is attributed to the lower dissociation energy of the N−H as compared with the N−D bond and to the enhanced tunneling efficiency of H atoms over D atoms through the barrier to dissociation. Similarly, the quantum yield for producing the $NH_2(\tilde{A},v_2' = 0)$ fragment is lower when an N−D bond must be cleaved in comparison to an N−H bond. Photodissociation of ND_2H by cleavage of an N−H bond leads to an $ND_2(\tilde{A})$ fragment with a much larger degree of vibrational excitation ($v_2' = 1,2$), accompanied by substantial rotation about the minor *b/c*-axes, than when an N−D bond is cleaved in the photodissociation of ND_3. The quantum yield for producing $NHD(\tilde{A})$ is larger for cleavage of an N−H bond from NH_2D than by cleavage of an N−D from ND_2H.

I. Introduction

Isotopic substitution of molecules is commonly used to probe quantum mechanical effects in the dynamics of photodissociation and chemical reactions.[1] While isotopic substitution does not modify the Born−Oppenheimer potential energy surfaces that are central to understanding the chemical event, it can dramatically alter the range of geometries sampled and thus lead to an alteration in the mechanism for the chemical process. Common examples of mechanistic information that can be probed by comparing hydrogen and deuterium substituted reactants include the role of tunneling through reaction barriers and the influence of the vibrational motion on the energy partitioning of the product species.

We have recently undertaken comprehensive studies of the photodissociation dynamics at an excitation wavelength of 193.3 nm of both NH_3 and ND_3,[2,3] probed by time-resolved Fourier transform infrared emission spectroscopy.[4−7] Specifically, we probed the vibrational and rotational energy partitioning in the electronically excited NH_2/ND_2 ($\tilde{A}^2A_1$) fragment. Comparison of the dynamics of the N−H and N−D bond cleavages in these two molecules suggests that a number of factors may be important in determining the mechanism of the dissociation. The Franck−Condon region of the multidimensional potential energy surface that is accessed in the excitation step has a pyramidal geometry and is bound classically;[8,9] the excitation wavelength of 193.3 nm corresponds to the preparation of NH_3 ($\tilde{A}^1A_2'',v_2 = 6$) and ND_3 ($\tilde{A}^1A_2'',v_2 = 7$).[10] As the parent molecule evolves away from the Franck−Condon region along the NH_3/ND_3 ν_2 bending coordinate, the barrier to N−H(D) bond cleavage decreases and at planar geometries the parent wave function is unbound and direct dissociation can occur.

The variation in the dissociation barrier with out-of-plane bending angle suggests that NH_3 and ND_3 may exhibit very different dynamics during bond cleavage. Not only are the symmetries of the initially excited bending vibrational wave functions different for these two parent molecules, but the absolute energy at which the barrier is sampled is different due to the change in zero-point energies of their respective ground states.[11] In addition, D atoms have a lower tunneling efficiency than H atoms, and it might be expected that this would influence the barrier region sampled during the dissociation. Measurements of the electronic absorption line widths have shown that NH_3 ($\tilde{A}^1A_2'',v_2 = 6$) has a lifetime of approximately 20 fs in the Franck−Condon region, while that for ND_3 ($\tilde{A}^1A_2'',v_2 = 7$) is ∼200 fs.[10] It has been suggested that the short lifetime of electronically excited NH_3 may be due not only to dissociations by tunneling but also to indirect dissociation mediated by a Fermi resonance between the umbrella bending motion of the excited state and the symmetric stretch.[8] The coupling of energy into the symmetric stretch mode can lead directly to motion in the dissociation coordinate.

Not only are the Franck−Condon and barrier regions key to determining the mechanism of the bond cleavage, but once the

† Part of the special issue "C. Bradley Moore Festschrift".

‡ National Research Council Research Associate, National Institute of Standards and Technology.

§ Current address: Department of Chemistry, Campus Box 1134, Washington University, One Brookings Drive, Saint Louis, Missouri 63130-4899.

|| Staff member, Quantum Physics Division, National Institute of Standards and Technology.

10.1021/jp001065r CCC: $19.00
Published on Web 06/23/2000

bond has lengthened to more than 1.5 Å, branching between the ground and first electronic excited states of the product is governed by the competition between nonadiabatic and adiabatic dynamics.[8,9] Dissociation from the excited-state parent $NH_3(\tilde{A}^1A_2'')$ to the excited-state fragments $NH_2(\tilde{A}^2A_1)$ occurs adiabatically, while nonadiabatic dissociation leads to the ground-state fragments $NH_2(\tilde{X}^2B_1)$. Away from planarity, the symmetries of the ground and excited states of NH_3 are the same and lead to an avoided crossing. However, at a planar geometry the symmetries of the states are different and a conical intersection permits dissociation from the excited state parent directly to the ground-state fragments. Many experimental and theoretical studies have probed the influence of the conical intersection on the energy partitioning in the ground electronic state fragment.[8,9,11−19] Biesner et al. determined the electronic energy partitioning between the ground and excited-state fragments.[13] It was shown that the $NH_2(\tilde{A}^2A_1)/NH_2(\tilde{X}^2B_1)$ ratio was 0.48 for dissociation from $NH_3(\tilde{A}^1A_2'', v_2 = 6)$ while in stark contrast, no $ND_2(\tilde{A}^2A_1)$ was produced from the excitation of $ND_3(\tilde{A}^1A_2'', v_2 = 6)$.

Our earlier studies of the vibrational and rotational energy partitioning in the excited electronic state fragments NH_2 and ND_2 suggest factors that are important in determining the mechanisms for the adiabatic N−H and N−D bond cleavages. The rotational energy partitioned about the primary *a*-axis is bimodal for both the NH_2 and ND_2 fragments from their respective parents, peaking at high K_a' ($K_a' = 5$ for NH_2 and $K_a' = 7$ for ND_2), near the energetic limit, and at the lowest K_a' observed. We have adopted the bent molecule notation in which the bending vibrational state $v_2' = 0$ is the lowest sublevel for each K_a'. Based on polarization studies by Mordaunt et al. for dissociation of ND_3 to the ND_2 ground electronic state fragments,[18] the low and high K_a'' states have been shown to arise from bond cleavages from significantly different geometries. The high rotational states are populated by dissociation from nonplanar geometries and the low rotational states by dissociation from planar geometries. This classical picture, shown schematically in Figure 1, can be used to explain the origin of the bimodal rotational distributions we observe for the excited electronic state products formed from the dissociation of NH_3 and ND_3. In addition, these different geometries sample different barrier heights, with nonplanar geometries requiring the H or D atom to tunnel through the barrier, while no barrier exists for planar dissociations.

Although we have qualitatively compared the bimodal distributions of NH_2 and ND_2 resulting from N−H and N−D bond cleavages, the exact origin of the bimodal rotational distribution remains elusive and these previous studies offer no unambiguous explanation for this trend in energy partitioning. In this work, the photodissociation dynamics of NH_2D and ND_2H, in which either the N−D or N−H bonds must be cleaved to give the NH_2 and ND_2 fragments, respectively, are examined. By this approach we can further elucidate the factors governing the partitioning of rotational excitation in the product and the dependence of this partitioning on the identity of the bond being cleaved.

The extent of bending vibrational excitation in the NH_2 and ND_2 products is remarkably different in the photodissociation of NH_3 and ND_3, respectively. While the ratio of $NH_2(\tilde{A}, v_2' = 0)/NH_2(\tilde{A}, v_2' = 1)$ was found to be 3:1, the same ratio in the dissociation of ND_3 was estimated to be 20:1. With the large energy available to the NH_2 and ND_2 fragments (14618 and 13723 cm^{-1}, respectively),[11] this dramatic change in the extent of vibrational excitation of the fragment cannot be attributed to an energetic factor. Instead, we have attributed it to the dynamics occurring during the bond cleavage, although currently the precise origin has not been determined. However, by studying the dissociation dynamics of NH_2D and ND_2H, it is hoped that the extent of vibrational excitation in the NH_2 and ND_2 fragments can be contrasted for N−H and N−D bond cleavages to give the same product fragment.

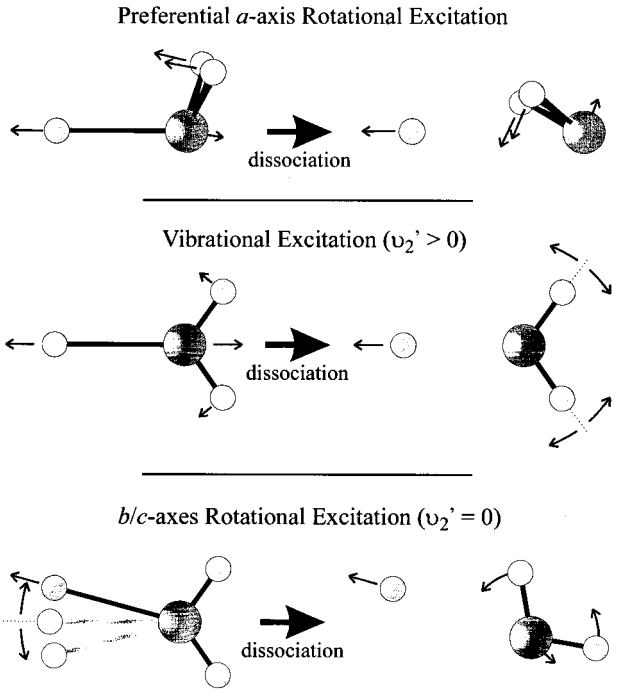

Figure 1. Schematic of the dissociation of ammonia with ν_2 bending excitation. The top panel illustrates how the rotational excitation about the *a*-axis is generated by a rotational torque about the *a*-axis of the $NH_2(\tilde{A})$ fragment as the N−H bond lengthens. For near-planar dissociation (middle panel), the departing H atom may give an impulsive kick to the N atom in the $NH_2(\tilde{A})$ product and thus induce bending excitation in the molecular fragment. A change in the equilibrium geometry (bottom panel) due to zero-point motion in the ν_4 coordinate, ±11° in NH_3, breaks the symmetry of the parent molecule and can classically generate a force about the $NH_2(\tilde{A})$ product *b*/*c*-axes.

The degree of rotational excitation about the minor *b*/*c*-axes of the fragment has been qualitatively rationalized by studying the photodissociation of NH_3 and ND_3.[2,3] If the parent molecules dissociate with C_{2v} symmetry, no rotational excitation about the *b*/*c*-axes is expected as no torque is exerted about the minor rotational axes. For room-temperature dissociation, the products with *b*/*c* rotational excitation are due to carryover of the parent rotational momentum into the products. In the jet-cooled NH_3 and ND_3 photodissociation studies, however, significantly more *b*/*c* rotational excitation is observed than is expected for a parent rotational temperature of 10 K. In addition, we found that the NH_2 fragment has a higher degree of *b*/*c* rotational excitation than ND_2. This *b*/*c* rotational excitation is attributed to the zero-point energy of the parent molecule in the ν_4 H−N−H scissors bending coordinate of the $NH_3(\tilde{A})$ predissociative state, in qualitative agreement with the predictions made by Dixon.[19] A schematic illustrating the origin of this excitation is shown in Figure 1. The departing atom moves out of the σ_v symmetry plane due to zero-point motion, breaking the C_{2v} symmetry of the parent molecule and leading to a torque about the minor-rotational axes as the bond cleaves. For NH_3 the zero-point motion in the ν_4 wagging motion was calculated to be ±11°.[19] The ND_3 parent has less zero-point energy than NH_3 and, thus, less zero-point bending amplitude. As the N−D bond lengthens

to dissociate, the D atom does not move as far out of the σ_v symmetry plane as the H atom in NH_3, and less torque can be exerted about the minor rotational axes, leading to a lower degree of excitation. Although we qualitatively understand the origin of this rotational excitation, probing the fragments from the dissociation of NH_2D and ND_2H should enable a more refined picture of this mechanism to be established.

Not only have we studied the photodissociation of NH_2D and ND_2H in order to further improve our understanding of the photodissociation dynamics, but probing the product species enables us to observe directly the competition between N−H and N−D bond cleavages from the same parent molecule. Probing the electronic state branching between the different competing channels in our experiment is equivalent to determining the relative proportions of the parent molecules dissociating through the specified channel adiabatically to the electronically excited state fragments. The possible electronically excited-state channels that can be probed are

$$NH_2D\ (\tilde{A}^1A_2'') \rightarrow NH_2(\tilde{A}^2A_1) + D\ (^2S) \quad (1)$$

$$NH_2D\ (\tilde{A}^1A_2'') \rightarrow NHD(\tilde{A}^2A_1) + H\ (^2S) \quad (2)$$

$$ND_2H\ (\tilde{A}^1A_2'') \rightarrow ND_2(\tilde{A}^2A_1) + H\ (^2S) \quad (3)$$

$$ND_2H\ (\tilde{A}^1A_2'') \rightarrow NHD(\tilde{A}^2A_1) + D\ (^2S) \quad (4)$$

By comparing the adiabatic branching ratios determined here with those measured by Mordaunt et al. for nonadiabatic dissociation to the ground electronic state products,[11] we probe the competition of nonadiabatic and adiabatic dynamics in the dissociation of NH_2D and ND_2H. Mordaunt et al. focused exclusively on the dissociation of the zero-point level and the first bending vibrational state of both $NH_2D(\tilde{A}^1A_2'')$ and $ND_2H(\tilde{A}^1A_2'')$.[11] These states lie energetically below the excited electronic product state asymptote and, thus, only the ground electronic state products are produced. For dissociation of $NH_2D(\tilde{A}^1A_2'')$ and $ND_2H(\tilde{A}^1A_2'')$, Mordaunt et al. concluded that the channels equivalent to 2 and 3, but for ground state fragments, dominate the dissociation dynamics. At such excitation energies, the parent molecules remain bound at all out-of-plane bending angles and the dissociation must be purely due to tunneling through the barrier. This explains the dominance of the N−H bond cleavage channels over N−D bond cleavage, along with the larger bond strength of the N−D over the N−H bond. They also concluded that for the reactions that yield $NHD(\tilde{X}^2B_1)$, for the equivalent of channels 2 and 4 but to ground-state fragments, significant internal conversion occurs with subsequent bond cleavage from unbound high-lying dissociative states of the ground electronic state of the parent molecule.

Probing the dissociation of $NH_2D(\tilde{A})$ and $ND_2H(\tilde{A})$ into electronically excited photofragments using FTIR emission spectroscopy requires the development of a spectral pattern recognition technique to isolate the spectral signatures of the fragments attributed to the dissociation of the two parent molecules.[20] This will be discussed in the following section II. Characterization of the electronic $\tilde{A} \leftarrow \tilde{X}$ absorption of the NH_2D and ND_2H species and their preparation is discussed in section III. A brief review of the experimental method, including the time-resolved Fourier transform infrared (FTIR) technique, is presented in section IV. Section V presents details of the spectroscopic analysis and of the product state distributions. Finally, we discuss in section VI the dynamics of the photodissociation of NH_2D and ND_2H.

II. Product State Spectral Pattern Recognition

Studying the photodissociation of NH_2D and ND_2H using emission-based techniques requires either state selective excitation of one parent molecule or a deconvolution of the product emission spectra following the simultaneous photofragmentation of all parent species into the components from each electronically excited fragment. Hydrogen atom exchange in ammonia is rapid and any attempt to chemically isolate the mixed deuterated parents leads only to an equilibrated mixture of all four parent molecules: NH_3, NH_2D, ND_2H, and ND_3. A broadband ArF excimer laser is used for these studies, and this leads to the unselective photodissociation of all four parent molecules simultaneously. Therefore, the product emission spectra consist of spectral signatures from six different photodissociation pathways, processes 1−4 above and processes 5 and 6

$$NH_3\ (\tilde{A}^1A_2'') \rightarrow NH_2(\tilde{A}^2A_1) + H\ (^2S) \quad (5)$$

$$ND_3\ (\tilde{A}^1A_2'') \rightarrow ND_2(\tilde{A}^2A_1) + D\ (^2S). \quad (6)$$

We have implemented a deconvolution technique that permits us to extract the product emission spectra arising from a specific parent molecule following the simultaneous photofragmentation of all parent species.[20] Our experiments probe only the excited electronic state fragments, so branching to the ground electronic state fragments is omitted from further discussion here. As the relative proportions of NH_3 and ND_3 that are initially mixed are varied, different equilibrium mixture compositions of the four parent species NH_3, NH_2D, ND_2H, and ND_3 are obtained. We previously characterized the composition of the equilibrated mixtures by mass spectrometry and the details are presented in ref 20.

Photodissociation of all four parent molecules simultaneously leads to product emission spectra that may contain concurrently the spectral signatures of the products from all six photodissociation pathways. The contribution of each spectral signature to the emission spectrum is dependent on a number of factors. These factors include the abundance of the respective parent molecule within the mixture of the four parent molecules being photodissociated, the relative absorption cross sections of the parent molecules and the quantum yield for formation of electronically excited photofragments. The relative transition strengths of the amidogen products (NH_2, ND_2, and NHD) and the total number of rovibrational product channels populated also determine the contribution of each spectral signature. Thus, mixtures rich in NH_2D may have strong spectral signatures for the products from channels 1 and 2. The intensities of all spectral features within the emission spectrum will be correlated with mixture composition in different ways, depending on the parent molecule from which they arise.

A cross-correlation spectral pattern recognition method was recently developed by Jacobson et al. and was extended by us to analyze dynamic product state distributions.[20−22] Not only does this method permit the easy identification and assignment of spectral features to specific reaction channels, but relative quantum yields for the various product channels can be estimated with only a limited knowledge and assignment of the spectroscopy of the product species.[20] To perform this quantum yield analysis, the relative absorption cross-sections of the different parent species must be known as well as the fractional compositions of the various mixtures used in the experiment.

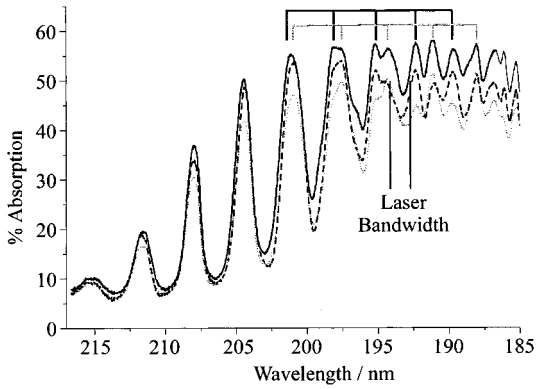

Figure 2. The $\tilde{A} \leftarrow \tilde{X}$ absorption spectra of NH_2D and ND_2H as measured with mixtures that contain NH_2D/ND_2H ratios of 1:1 (solid line), 2:1 (dotted gray line), and 1:2 (dashed black line). The absorption from NH_3 and ND_3 has been subtracted from all three spectra. Tic marks show the absorption features due to NH_2D (grey line) and ND_2H (black line).

We have applied this method for spectroscopic analysis to the study of the photodissociation dynamics of NH_2D and ND_2H, extracting the independent spectral signatures for the photodissociation channels 1−6 from the raw spectral data sets for nine different mixtures with differing parent molecule compositions. In addition, by measuring the $\tilde{A} \leftarrow \tilde{X}$ absorption spectra of the NH_2D and ND_2H species and the mixture compositions by mass spectrometry, we have been able to determine the relative quantum yields for channels 1−6. Important details of the product state spectral cross-correlation analysis are given in the sections that follow, although for a complete discussion of this pattern recognition technique, the reader is referred to our earlier paper.[20]

III. Preparation and Characterization of NH_2D and ND_2H

An equilibrium mixture of NH_3, NH_2D, ND_2H, and ND_3 is rapidly formed on mixing NH_3 and ND_3. To apply the product state spectral cross-correlation analysis, a well-defined variable must be systematically altered, permitting correlations of the spectral features to be observed. The variable used in this study is the initial mixing ratio of NH_3 to ND_3, which determines the composition of the equilibrium mixture. In a previous paper we showed details of how this mixing ratio leads to particular equilibrium mixture compositions, as characterized by mass spectrometry.[20]

A further method for characterizing the equilibrated mixture is by ultraviolet (UV) absorption, which enables us to also investigate the $\tilde{A} \leftarrow \tilde{X}$ absorption spectroscopy of the NH_2D and ND_2H species. A gas cell with a path length of approximately 10 cm was filled with 100 Torr of the mixture of NH_3, NH_2D, ND_2H, and ND_3. The UV absorption spectrum was obtained at room temperature in the spectral range 220−190 nm. The absorption spectra of pure NH_3 and ND_3 were also obtained and subtracted from the raw $\tilde{A} \leftarrow \tilde{X}$ absorption spectra of the mixture, using the mixture compositions determined by mass spectrometry. The resulting spectra for three mixture compositions, which include only the absorptions due to NH_2D and ND_2H, are shown in Figure 2.

The $\tilde{A} \leftarrow \tilde{X}$ absorption spectra show a progression in the ν_2 bending vibration of the $\tilde{A}$ state, denoted by 2_0^n, where the superscript denotes the vibrational level of the excited electronic state and the subscript the vibrational level of the ground electronic state. This is analogous to the progressions observed in the $\tilde{A} \leftarrow \tilde{X}$ absorption spectra of both NH_3 and ND_3.[10,23,24] The band origins 2_0^0 are in agreement with earlier studies and lie at ∼215 nm.[11,15,16] With the studies being performed at room temperature, the band origins are not resolved for the NH_2D and ND_2H species. As the vibrational state accessed in the upper electronic state increases, the individual bands for the two species become resolved. At the excitation wavelength used in the photodissociation experiments of 193.3 nm (51730 cm^{-1}) and with an approximately 200 cm^{-1} energy bandwidth, the 2_0^7 transition of ND_2H will be excited, with the peak in absorption occurring at 51985 cm^{-1}. NH_2D will be excited by the 2_0^6 transition, which has a peak absorption at 51455 cm^{-1}.

A detailed analysis of the $\tilde{A} \leftarrow \tilde{X}$ absorption spectra of these species is beyond the scope of this work. However, the relative absorption cross-sections of NH_2D and ND_2H in the frequency bandwidth of the laser must be estimated to determine the relative branching ratios of the product photodissociation channels. To estimate the relative absorption cross-sections, the absorption spectra of the mixtures were integrated in the range 51530 cm^{-1} to 51830 cm^{-1}. Knowing the relative compositions of the mixtures used, it was then possible to estimate the relative absorption cross-sections of NH_2D and ND_2H in the wavelength range crucial to the photodissociation experiments. These were then compared with the absorption cross-sections of NH_3 and ND_3. The NH_3 $\tilde{A} \leftarrow \tilde{X}$ 2_0^6 absorption cross-section has been measured at 193 nm to be $\sim 1.7 \times 10^{-17}$ cm^2.[25] Relative to a cross-section set to unity for absorption by NH_3, the relative absorption cross-sections at room temperature at 193 nm for NH_2D, ND_2H, and ND_3 are 0.69, 1.2, and 0.86, respectively. No absorption spectra were recorded under jet-cooled conditions, and the relative absorption cross-sections may change dramatically when the parent molecule is cooled.

IV. Experimental Section

A detailed description of the experimental apparatus has been given in a previous publication and only a concise summary is presented here.[2] A pulsed ArF excimer laser is synchronized to the scan of a commercial FTIR. The 193 nm laser emission initiates the photodissociation event producing electronically excited $NH_2/NHD/ND_2$ fragments, and the electronic emission ($\tilde{A}^2A_1 \rightarrow \tilde{X}^2B_1$) from these products is imaged into the FTIR.

The photodissociation experiments were performed with a thermal room-temperature flow of the mixture of NH_3, NH_2D, ND_2H, and ND_3 and with a jet-cooled expansion. In the latter case, the ammonia mixture was prediluted in a helium buffer gas. A piezoelectric pulsed valve, similar in design to that of Proch and Trickl,[26] with a nozzle diameter of 750 μm, was used to cool the parent species to a temperature estimated to be 10 K. Comprehensive tests were performed to ensure that contributions from the photolysis of clusters of parent species was negligible. These studies have been presented previously and only the details important to the measurements made here will be repeated.[2] It is important to ensure that the dilution of ammonia in a helium buffer gas and the backing pressure of the pulsed valve are sufficiently low to avoid clustering of the parent molecules. Our previous studies on the photodissociation of NH_3 and ND_3 used backing pressures of 67 kPa and dilutions of 1% and 2% ammonia in helium.[2] While these conditions yielded a sufficiently high signal-to-noise ratio for the study of these single parent species, in the experiments presented here, four parent molecules are undergoing simultaneous photodissociation. This requires that the stringent condition imposed on the concentration must be marginally relaxed. In all of the studies presented here, a backing pressure of 67 kPa was used

as before, but the dilution used is now 5% in helium. While this leads to an increase in the uncertainty of the populations of the product states by up to 10% according to our earlier studies, the improvement in the signal-to-noise ratio that results outweighs the introduction of such a small systematic error. In addition, the product state distributions determined for NH_3 and ND_3 in these current experiments were within the error bars of the measurements we have published recently. Similar experiments with an expansion of NH_3 in Ar and an orifice of 1 mm showed that the rotational temperature of the jet-cooled parent molecule was <10 K.[27,28] We hereafter refer to the parent temperature of the ammonia species as 10 K.

The photodissociation event is initiated by an ArF excimer laser operating at a repetition rate of 140 Hz. The triggering of the laser and the pulsed valve expansion in the jet-cooled experiments are synchronized to the scan of the moving mirror of a commercial continuous scan FTIR spectrometer in the same manner discussed in a previous publication.[2] The laser fluence within the photodissociation region is measured to be ∼75 mJ/cm^2. The photolysis beam intersects the room-temperature thermal flow or the jet-cooled expansion of the ammonia mixture in a vacuum chamber that is evacuated by a 300 L/s roots blower pump, backed by an 80 L/s mechanical pump. Emission from the electronically excited photofragments is imaged into the FTIR spectrometer from the gas expansion with a CaF_2 lens/Al mirror-telescope arrangement. The modulated emission is detected by one of two detectors. The $NH_2/ND_2/NHD(\tilde{A}^2A_1 \rightarrow \tilde{X}^2B_1)$ electronic emission is in the spectral range 6000 to 15000 cm^{-1}. To acquire a complete spectrum over this broad frequency range, the experiment must be repeated under identical experimental conditions with two detectors, an InSb detector for the range 6000 to 12000 cm^{-1} and a Si avalanche photodiode for the range 10000 to 15000 cm^{-1}. A second identical detector is used to monitor the total unmodulated emission intensity, and the modulated signal is thus corrected for variations in the laser power and gas flow using this second normalization channel. A complete spectrum with a Nyquist frequency of 15798 cm^{-1} is acquired with a spectral resolution of 0.2 cm^{-1}. A total of between 16 and 24 coadditions are recorded for each spectrum.

A time-resolved history of the emitting photofragments over the first 20 μs after their nascent production is acquired by up to eight boxcar integrator gates. Analysis of the time-resolved spectra shows that no significant quenching of the product fragments occurs within the first 200 ns to 2 μs after their production. Thus, all of the product state distributions quoted below are obtained within the first 2 μs after the photofragmentation and are assumed to be nascent.

V. Spectroscopic Analysis

The spectroscopic analysis of the photofragment emission involves three stages. First, the spectral signatures for each of the photofragmentation channels 1−6 must be identified in the raw spectral data and extracted by the product state spectral pattern recognition method. Once isolated, the product state distributions for each of the photofragmentation channels must be determined after assignment of the spectral features. Finally, the available information is used to estimate the relative quantum yields for the different photodissociation channels. Each of these stages will be discussed in turn.

Product State Spectral Pattern Extraction. The mechanism for extraction of the product state spectral patterns has been presented in detail in a previous publication.[20] Briefly, the analysis consists of forming recursion maps, which take the raw data sets for the nine experiments performed with different mixture compositions and form plots of the intensity from one experiment versus the intensity from another, instead of intensity versus frequency. This procedure requires an accurate and identical frequency calibration from one experiment to another and a reproducible intensity axis. The recursion map immediately leads to the separation of the spectral features present in the raw data sets into sets of spectral features that correlate in an identical manner with composition.[21,22] Each set of spectral features is termed a spectral pattern and corresponds to a ray of points emanating from the origin. The assignment of these different spectral patterns to specific reaction channels is not straightforward, but a procedure for establishing the assignment is given in our previous publication.[20]

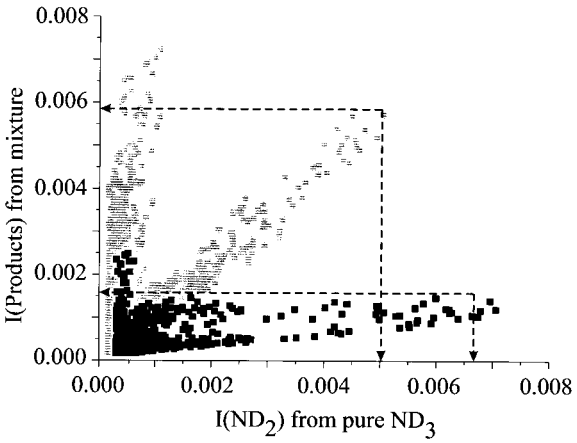

Figure 3. Correlation plot of the emission spectra from two photodissociation experiments: the photodissociation of pure ND_3 (horizontal axis) and the photodissociation of a mixture composed of approximately 40% NH_2D, 40% ND_2H, 10% NH_3, and 10% ND_3 (vertical axis). Two correlation plots are overlaid to illustrate how the correlations can dramatically change on jet-cooling the sample (black squares) compared to photodissociation at room temperature (grey squares).

An example of a recursion map is illustrated in Figure 3. The correlation between only two experiments is shown. Experiments were performed for nine mixture compositions in a room temperature flow and seven mixture compositions for the jet-cooled expansion. Thus, the full data sets for these two different experiments involve 9 and 7 dimensions, respectively. Figure 3 also shows how the recursion map changes for two mixtures when photodissociated at the two different temperatures, identical in composition in both the room-temperature and jet-cooled dissociations. Two rays are observed in the recursion map for room temperature dissociation, each with a similar number of spectral features and with similar intensities. In the jet-cooled dissociation, the ray closest to the horizontal axis now dominates and is much more intense than the ray close to the vertical axis. Whatever the identity of the parent species giving rise to these rays, they represent product fragments coming from two different sets of parent species. Since one diminishes in strength relative to the other upon jet-cooling, the data suggest that the relative absorption cross-sections for the different parent species change dramatically on jet-cooling, relative to room temperature. A reduction in the absorption cross-section at 193.3 nm upon jet-cooling the parent molecule reduces the yield of product fragments in the photodissociation and, thus, the intensity of the ray in the recursion map.

Once the recursion maps have been made, the spectral features are grouped together in sets, specified by a direction in 9(7)-dimensional space, and each set corresponds to features that are correlated with mixture composition in a similar way. All that remains is to locate the spectral patterns in 9(7)-dimensional space and to extract the spectral features that occur in each

pattern. This is achieved by applying the techniques developed by Jacobson et al. for locating the rays, or spectral patterns, and then for extracting the patterns.[21,22] The pattern extraction is applied twice, once for the room-temperature dissociation spectra and then for the jet-cooled spectra. A detailed discussion of the procedure adopted is presented in our previous publication along with an identification of the patterns extracted.[20] It is important to note that, surprisingly, no identifiable pattern is extracted for the photofragment NHD.

Spectroscopy and Product State Analysis. In our previous publications,[2,3] we have described in detail the spectroscopic assignment and analysis of both the NH_2 and ND_2 ($\tilde{A}^2A_1 \rightarrow \tilde{X}^2B_1$) electronic emission. The electronic selection rules follow those of a symmetric prolate top; the change in the total rotational angular momentum, $\Delta N = \pm 1$, equals the change in rotational quanta about the major *a*-axis, i.e., $\Delta N = \Delta K_a = \pm 1$. Rotational angular momenta about the minor *b*/*c*-axes is given by those values of N' for which $N' > K_a'$. Using the notation for absorption, the emission spectrum is dominated by vibrational bands with ${}^{P}P(N'',K_a'')$ and ${}^{R}R(N'',K_a'')$ rotational lines. The P and R superscripts refer to $\Delta K_a = -1$ and $\Delta K_a = +1$, respectively, and the *P* and *R* branches refer to $\Delta N = -1$ and $\Delta N = +1$. Each rotational transition is further split by spin-rotation coupling into two components, $F_1 \rightarrow F_1$ and $F_2 \rightarrow F_2$. The observed spectral lines are attributed to rotational transitions within the vibrational bands originating from $v_2' = 0$ (2_0^0, 2_1^0, 2_2^0, 2_3^0, 2_4^0) where the superscript denotes the vibrational level of the excited electronic state and the subscript that of the ground state. The spectroscopy of NH_2 ($\tilde{A}^2A_1 \rightarrow \tilde{X}^2B_1$) is well characterized,[29−34] and the transitions relevant to this study for ND_2 ($\tilde{A}^2A_1 \rightarrow \tilde{X}^2B_1$) have recently been assigned by us.[3] In Figure 4 we show a section of the emission spectra from the photodissociation of a mixture, one from the room-temperature dissociation and one from the jet-cooled study. This illustrates the simplification of the spectra upon reducing the parent rotational energy by jet-cooling.

The relative populations, $n(N', K_a')$, found within each NH_2/$ND_2(\tilde{A})$ rovibrational level are determined[35] from the intensities, *I*, of the ${}^{P}P(N'',K_a'')$ emission lines, the transition frequencies, ν, Hönl−London factors, $A_{K_a'',N''}$, and theoretically predicted rovibronic transition moments, *R*, according to

$$n(N', K_a') = \frac{I}{A_{K_a'',N''}|R|^2\nu^3} \tag{7}$$

The Hönl−London factors, $A_{K_a''N''}$, appropriate for a perpendicular transition are used[35]

$$A_{K_a'',N''} = \frac{(N'' - 1 + K_a'')(N'' + K_a'')}{K_a''(2K_a'' + 1)} \tag{8}$$

and the averages of the F_1 and F_2 intensities for each transition are used.

The vibronic intensity factors, *R*, for the spectroscopy of NH_2 have been calculated and are included in the analysis.[36] However, these factors are not known for ND_2 and, thus, in what follows the product state distributions for ND_2 are only qualitatively correct and for a quantitative analysis a correction for *R* is necessary. While the ND_2 product state distribution produced by the N−H and N−D bond cleavages in ND_2H and ND_3 can be directly compared, no direct comparison can be made between the distributions obtained for NH_2 and ND_2. By analogy with the analysis performed on the fragment NH_2 from NH_3, correction by the vibronic intensity factors is not expected to change the qualitative trends and conclusions of this work. A detailed discussion of this conclusion is presented in our previous paper on the photodissociation dynamics of ND_3.[3]

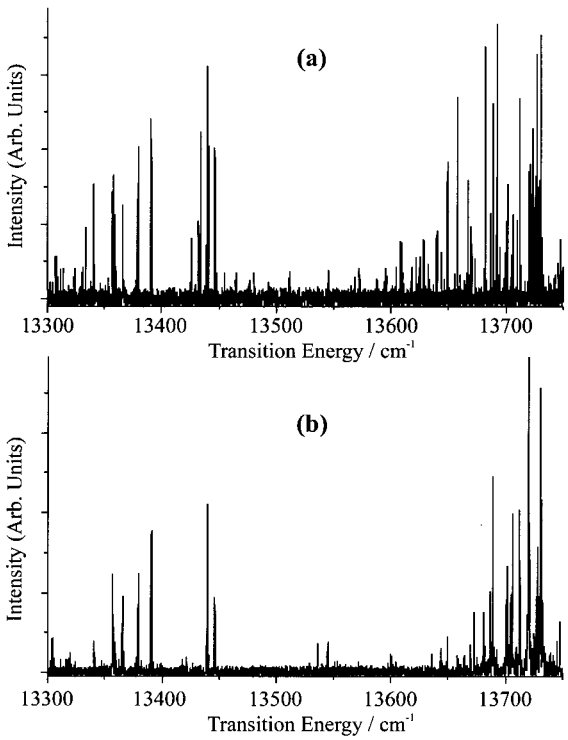

Figure 4. A section of the product emission spectrum of $NH_2(\tilde{A}^2A_1)$, $ND_2(\tilde{A}^2A_1)$, and $NHD(\tilde{A}^2A_1)$ from the photodissociation of a mixture containing approximately 0% NH_3, 35% NH_2D, 45% ND_2H, and 20% ND_3. Panel (a) is for a room-temperature dissociation and (b) is for jet-cooled. Note the significant simplification of the spectra on jet-cooling the parent molecule. The R-band centered at 13450 cm^{-1} is assigned to ND_2 fragment transitions from $2_0^0\ {}^{R}R(8)$ while the band centered at 13700 cm^{-1} is assigned to transitions from 2_0^1. The rotational structure in each band reflects the degree of rotation about the minor *b*/*c*-axes. This illustrates the considerably higher degree of $N' > K_a'$ rotation in the $ND_2(\tilde{A}, v_2' = 1)$ fragment from the dissociation of ND_2H, than that in the $ND_2(\tilde{A}, v_2' = 0)$ product from the photodissociation of both ND_3 and ND_2H.

The $N' = K_a'$, $v_2' = 0$ population distributions for $ND_2(\tilde{A})$ produced from cleavage of an N−H and an N−D bond (ND_2H and ND_3 respectively) are shown for comparison in Figure 5a and b. Figure 5a illustrates the product distribution from jet-cooled dissociation and Figure 5b from room-temperature dissociation. The error bars reflect the uncertainty in the rotational state populations when estimated from up to four different vibrational bands and are thus determined by the signal-to-noise ratio in the emission spectra, following the procedures outlined in ref 37. As discussed in our previous publication,[20] a single pattern is not extracted for ND_3 fragmentation and another for ND_2H. Instead, the spectral features are distributed between two different spectral patterns, one incorporating those features that correlate in approximately the same way, within the signal-to-noise of the experiment, with the sum of the fractional compositions in the mixture of ND_3 and ND_2H. The remaining states are correlated with the fractional composition of only ND_2H in the mixture. These states correspond to the highest $N' = K_a'$ levels, where the signal intensity is close to the signal-to-noise limit for ND_3 dissociation, but much enhanced for ND_2H dissociation. This is principally due to the increased available energy for ND_2 from ND_2H (14433 cm^{-1}) compared with ND_3 (13723 cm^{-1}), permitting significant population in $N' = K_a' = 8$ and 9. It should be noted that the

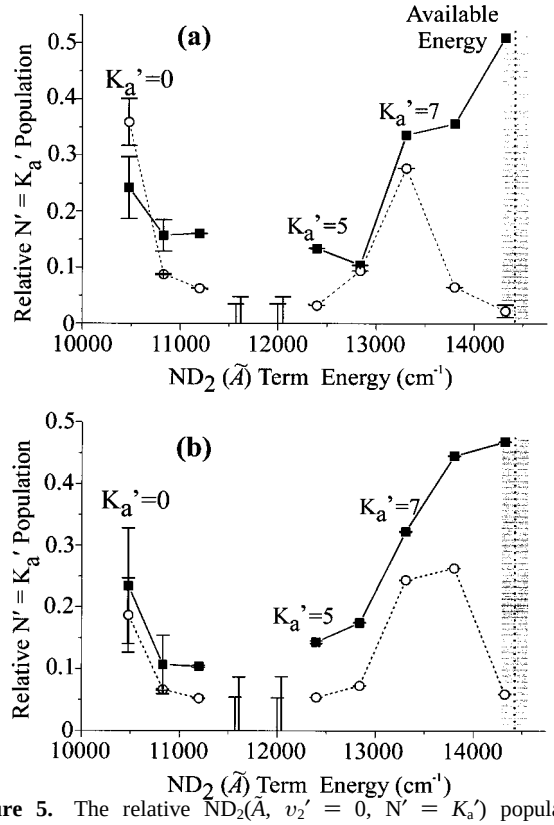

Figure 5. The relative $ND_2(\tilde{A}, v_2' = 0, N' = K_a')$ population distributions obtained by the 193.3 nm photolysis of ND_3 (open circles) and ND_2H (filled squares). Panel (a) illustrates the distributions from the jet-cooled photodissociation and panel (b) from the room-temperature photodissociation. Note the trend to higher populations in high K_a' states when ND_2H is dissociated compared with ND_3. The highest population for ND_2 from ND_2H is found in the highest accessible $N' = K_a' = 9$ state. The product state distribution for the dissociation of ND_2H is scaled so that the total population reflects the enhanced quantum yield for producing the $ND_2(\tilde{A}, v_2' = 0, N' = K_a')$ fragment from the photodissociation of ND_2H compared with ND_3, as reported in Table 1. The maximum available energy is shown for the ND_2 fragment in the dissociation of ND_2H, with a bandwidth that denotes the laser wavelength bandwidth. The maximum available energy for the ND_2 fragment in the dissociation of ND_3 is 13723 cm^{-1}. Note that the $N' = K_a' = 3$ and 4 states are not observed within the signal-to-noise ratio of our experiments, and maximum limiting error bars are displayed as determined from the signal-to-noise ratio of the emission spectra at only approximate internal energies.

relative quantum yield for producing $ND_2(\tilde{A}, N' = K_a', v_2' = 0)$ from ND_2H compared with ND_3 is taken account of in this figure, as discussed in the following section. Once all of the ND_2 spectral features are identified and the product state distribution calculated, a check of the extraction method was performed by analyzing the same ND_2 spectral features in the raw spectrum obtained for the mixture with the largest ND_2H/ND_3 ratio. With the larger absorption cross-section of ND_2H over ND_3 and the dominance by 3:1 of ND_2H over ND_3 in the mixture, the agreement between the two product state distributions confirms the validity of the pattern extraction method.

Both NH_3 and NH_2D can dissociate to yield $NH_2(\tilde{A})$. However, the NH_2 fragment pattern extracted correlates approximately with the fractional composition of just NH_3 in the mixture. Once the NH_2 features in the raw spectra are analyzed from the mixture richest in NH_2D, a weakness in the pattern recognition method is discovered. This weakness is shown in Figure 6. Although it is suggested from the pattern recognition method that the NH_2 spectral features come only from NH_3, Figure 6 shows that the fragmentation of a mixture rich in NH_2D

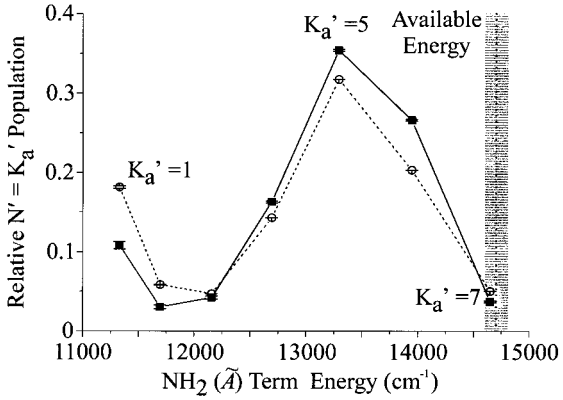

Figure 6. The relative $NH_2(\tilde{A}, v_2' = 0, N' = K_a')$ population distributions obtained by the 193.3 nm photolysis of jet-cooled pure NH_3 in He (filled squares) and a mixture of NH_3/NH_2D in He with an approximate ratio of 1:2 (open circles). The maximum available energy is shown for the NH_2 fragment in the dissociation of NH_3, with a bandwidth that denotes the laser wavelength bandwidth.

by process (1) leads to an $NH_2(\tilde{A})$ product state distribution that differs only marginally from that for NH_3. Figure 6 does permit the maximum change in the NH_2 distribution from that for pure NH_3 to be extracted for any of the experiments performed. It must therefore be concluded that to resolve such a minor change in the product state distribution, either a higher signal-to-noise ratio in the spectra has to be achieved, or more mixture compositions that illustrate this minor change in distribution must be used. As noted in the following section, the quantum yield for the photodissociation of NH_2D to electronically excited fragments is much smaller than that for NH_3 and the absorption cross-section of NH_2D is much lower than that of NH_3. These factors conspire to ensure that the spectral signatures of NH_2 produced from NH_2D are only very weak and greatly dominated by those from NH_3, making it difficult to discern the contribution to the NH_2 signal from NH_2D. In all that follows, when the NH_2D product state distribution is discussed it will only be derived by comparing the difference in dissociating pure NH_3 and the mixture containing both NH_3 and NH_2D in the jet-cooled dissociation experiment. The population distributions are not compared for thermal room-temperature dissociation as the signal-to-noise ratios are not sufficient for conclusions to be drawn about the differences in the population distributions from NH_3 and the mixture.

The integrated vibrational band intensities over all rotational transitions for the NH_2 and ND_2 products from the four parent molecules are presented in Figure 7, with the values for $v_2' = 1$ and 2 shown relative only to that in $v_2' = 0$ for each of the different parent molecule dissociations. A direct population comparison is prohibited, as the vibronic intensity factors for ND_2 are not known. All of the parent species give products with a similar ratio of populations in $(\tilde{A}, v_2' = 0):(\tilde{A}, v_2' = 1)$, apart from ND_3. The low level of vibrational excitation in the ND_2 product has been discussed in a previous publication.[3] By contrast the ND_2 product from ND_2H has a much higher level of vibrational excitation. Indeed, significant population is seen in ND_2 $(\tilde{A}, v_2' = 2)$. It should be noted here, however, that accompanying this large degree of vibrational excitation in the ND_2 product from ND_2H is a large degree of rotational excitation about the minor *b/c*-axes. In contrast to the rotational excitation in NH_2 from NH_3, the ND_2 rotational transitions from $N' > K_a'$ levels following the photolysis of ND_2H do not appear to obey the selection rules of a prolate symmetric rotor. The rotational structure in the spectra, as shown in Figure 4 for the

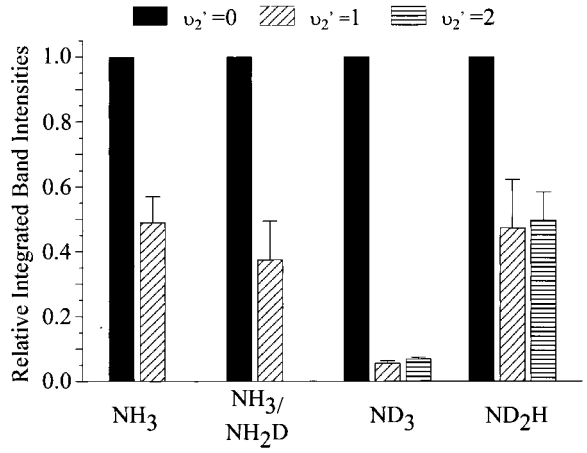

Figure 7. Vibrational excitation of NH_2 and ND_2 produced in the photodissociation of NH_3 and NH_2D, and ND_2H and ND_3. The vibrational branching is estimated by comparing the relative integrated band intensities over all rotational transitions of the upper vibrational product states compared with ($\tilde{A}$, $v_2' = 0$, $N' = K_a'$).

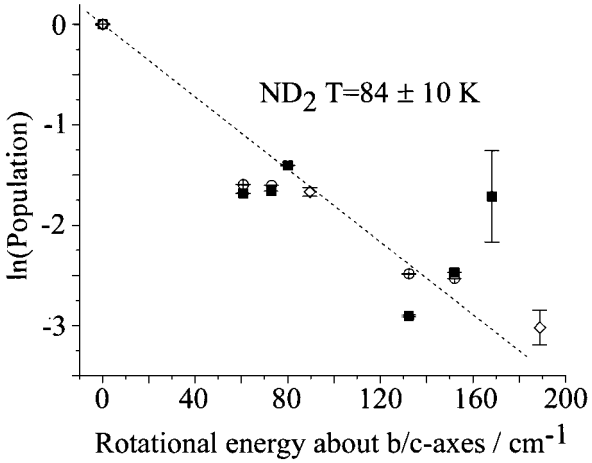

Figure 8. Boltzmann-type plots of $ND_2(\tilde{A}, v_2' = 0)$ $N' \geq K_a'$ populations following photolysis of jet-cooled ND_3 (filled squares) and ND_2H ($K_a' = 7$ and 8, open circles; $K_a' = 9$, open diamonds). No difference in the level of excitation of the $ND_2(\tilde{A}, v_2' = 0)$ fragment is observed within the signal-to-noise ratio of the experiments presented here. The data are best fit by a Boltzmann temperature of 84 ± 10 K.

vibrational band centered around 13700 cm^{-1}, is complex and an analysis is beyond the scope of this work.

Although the degree of $N' > K_a'$ excitation in the ND_2 ($\tilde{A}$,v_2' = 1, 2) product from ND_2H is large, this is not true for the $ND_2(\tilde{A},v_2' = 0)$ levels. This is shown in Figure 8. The Boltzmann temperature for rotation about the minor *b/c*-axes with $v_2' = 0$ appears to be very similar to that for ND_2 from ND_3. This suggests that these different vibrational levels of the ND_2 product from ND_2H may have very different dynamic origins.

No direct evidence for NHD($\tilde{A}$) in the product state spectral patterns is observed. However, as discussed in our previous publication,[20] the residuals remaining in the spectral data sets following the extraction of the strong NH_2 and ND_2 patterns reveal that a small amount of NHD($\tilde{A}$) is produced. The integrated band intensity of these NHD residuals is illustrated in Figure 9 with variation in mixture composition. This shows that once the absorption cross-sections of the parent species are accounted for, NH_2D is the most significant producer of NHD($\tilde{A}$). For the mixture with approximately equal proportions of NH_2D and ND_2H, approximately equal amounts of NHD($\tilde{A}$) are produced from the two parent species. This suggests that

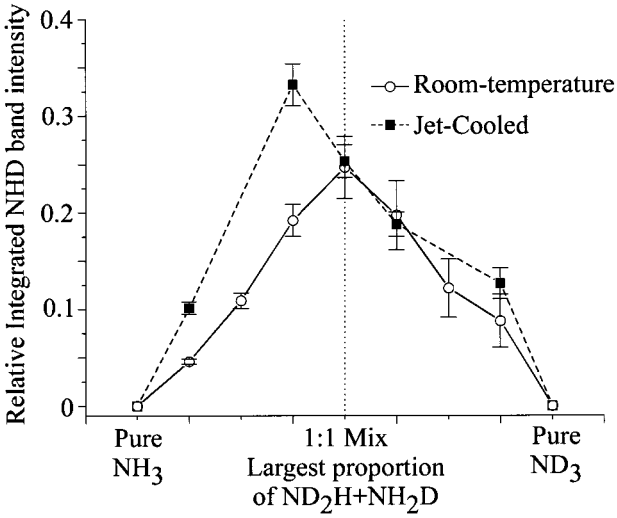

Figure 9. Variation in the integrated NHD emission band intensity with mixture composition, showing that the maximum NHD($\tilde{A}$) yield occurs on jet-cooled dissociation of the mixtures richest in NH_2D.

the quantum yield for producing electronically excited NHD from NH_2D is approximately twice that from ND_2H.

Estimation of the Relative Quantum Yields for N−H and N−D Bond Cleavages. In a recent publication we showed that it is possible to estimate the relative quantum yields for the different photodissociation pathways.[20] By considering one spectral feature from ND_2, the peak intensity is composed of a certain proportion from the dissociation of ND_3 and a certain proportion from ND_2H. The relative contributions of these two channels to the peak intensity is dependent on the relative fractions of the two parent species in the mixture, χ(M), the relative absorption cross-sections of the two species, σ(M), and the relative electronically excited-state quantum yields for the two dissociation pathways, $\Phi(ND_2 \leftarrow M)$.

$$P(ND_2) \propto \chi(ND_3)\,\sigma(ND_3)\,\Phi(ND_2 \leftarrow ND_3) + \chi(ND_2H)\,\sigma(ND_2H)\,\Phi(ND_2 \leftarrow ND_2H) \quad (9)$$

For each mixture, we have determined the fractional compositions of all of the mixtures and estimated the relative absorption cross-sections of the different parent species at room temperature. By knowing these, expressions can be derived that enable the relative quantum yields to be calculated. Geometrically, this corresponds to predicting the direction of each spectral pattern in the 9(7)-dimensional space. The deviation of each pattern from the predicted direction determines the relative quantum yields for the different photodissociation pathways.[20]

Relative quantum yields have been estimated for dissociation at room temperature for the processes: $\Phi[ND_2(\tilde{A}, N' = K_a', v_2' = 0) \leftarrow ND_2H]/\Phi[ND_2(\tilde{A}, N' = K_a', v_2' = 0) \leftarrow ND_3]$, $\Phi[ND_2(\tilde{A}, N' = K_a', v_2' = 1, 2) \leftarrow ND_2H]/\Phi[ND_2(\tilde{A}, N' = K_a', v_2' = 1, 2) \leftarrow ND_3]$, and $\Phi[NH_2(\tilde{A}, N' = K_a', v_2' = 0) \leftarrow NH_2D]/\Phi[NH_2(\tilde{A}, N' = K_a', v_2' = 0) \leftarrow NH_3]$. A direct comparison of the different product channels, for example processes 1 and 2, cannot be made as the vibronic intensity factors for ND_2 and NHD are not known. Thus, in Table 1, the relative quantum yields can be only compared across the rows, and not down the columns.

VI. Discussion

We undertook the experimental work presented here to further refine our understanding of the adiabatic dissociation of

TABLE 1: Relative $\tilde{A}$ State Quantum Yields of Products from the Room Temperature Photodissociation of NH_3, NH_2D, ND_2H, and ND_3[a]

	parent molecule			
product fragment	NH_3	NH_2D	ND_2H	ND_3
$NH_2(v_2' = 0, 1, 2)$	1	0.4 ± 0.2		
NHD		1.4 ± 0.2	1.0 ± 0.2	
$ND_2(v_2' = 0)$			2.0 ± 0.5	1
$ND_2(v_2' = 1, 2)$			6.0 ± 0.5	1

[a] Relative quantum yields should be compared along rows only. For comparisons to be made down columns, the difference in transition moments for the sets of transitions occurring from the different product species would have to be accounted for. These transition moments are currently unknown for NHD and ND_2.

ammonia to excited electronic fragments. From our earlier studies on the photodissociation dynamics of NH_3 and ND_3, we concluded that a number of factors were important in determining the mechanism of the bond cleavage.[2,3] To summarize the discussion of the dissociation mechanism as presented in the Introduction of this paper, the Franck−Condon region accessed on the excited state surface has a pyramidal geometry and is classically bound. As the molecule undergoes a bending vibration, the dissociation barrier diminishes and at planar geometries the molecule can dissociate directly. The barrier region sampled by the dissociating molecule is determined by the excited vibrational state wave function, and this is considered to have a major impact on the energy partitioning in the product, as illustrated in Figure 1. Once the barrier region is surpassed, the competition between dissociation to the ground and first electronic excited states must be considered. Dissociation trajectories that proceed by the lengthening of the N−H bond in planar geometries would have a greater probability for nonadiabatic dissociation to the ground state by passage through the conical intersection. Thus, by probing the excited electronic state fragments, we might expect to see predominantly those dissociations that involve the sampling of large out-of-plane bend angles during the bond cleavage. In what follows we will discuss the product state distributions from the photodissociation of NH_2D and ND_2H and the implications of these observations for the dissociation mechanism. However, this discussion is intended to present only a qualitative understanding of the dissociation mechanism. A comprehensive understanding of the adiabatic dissociation pathway will require additional theoretical calculations.

The rotational partitioning about the major *a*-axis has now been shown to be bimodal for all four of the parent molecule dissociations when yielding the C_{2v} symmetric product species $NH_2(\tilde{A})$ and $ND_2(\tilde{A})$.[2,3] It is instructive to compare the $N' = K_a'$ rotational distributions of $NH_2(\tilde{A})$ when cleaving N−H (NH_3) and N−D (NH_2D) bonds, and $ND_2(\tilde{A})$ when cleaving N−H (ND_2H) and N−D (ND_3) bonds. In both comparisons, the qualitative changes in the bimodal distributions are in agreement. Cleavage of an N−D bond leads to an enhancement in the population of the low K_a' states, while cleavage of an N−H bond leads to an enhancement in the population of the high K_a' states, an example of which is shown in Figure 5. We have suggested in our previous publications that the competition between planar and nonplanar dissociation pathways may lead to the bimodality of the rotational distribution. This is supported by the polarization studies of Mordaunt et al.,[18] who showed that the high K_a'' states arise from nonplanar dissociation geometries and the low K_a'' states from planar geometries of $ND_3(\tilde{A}, v_2 = 0)$ to give the ground electronic state fragment. It is also possible that with the change in vibrational constants for different parent molecules, the vibrational wave function leading to dissociation may significantly change if any favorable IVR processes or Fermi resonances exist.

One possible explanation for the bimodal rotational distributions may be the enhanced tunneling efficiency of H atoms over D atoms. This may lead to an increased rate of nonplanar tunneling dissociations for cleavage of an N−H bond rather than an N−D bond. Thus, a higher degree of rotational excitation in the product is produced because the barriers at larger out-of-plane bending angles are overcome during the tunneling dissociation of the H atom. In support of this hypothesis and the role of tunneling, the relative quantum yields for producing specific electronically excited product species, as shown in Table 1, increase dramatically when an N−H bond is cleaved instead of an N−D bond. It follows that this should at least partially reflect the enhanced tunneling of H atoms over D atoms, leading adiabatically to the $\tilde{A}$ state fragment.

In addition, the lower zero-point energy of the deuterated parent species[11] suggests that the excitation step leads to an excited parent molecule that lies lower in energy on the excited state potential energy surface. Therefore, the deuterated parent molecules remain classically bound at smaller out-of-plane bending angles and the barrier to dissociation greatly inhibits the dissociation. With the reduced tunneling efficiency of D atoms over H atoms, this may confine the direct dissociation to a much narrower range of bending angles, a range of geometries closer to the geometry of the conical intersection as the N−D bond lengthens. The work of Biesner et al. showed that the ratio of $NH_2(\tilde{A}^2A_1)/NH_2(\tilde{X}^2B_1)$ was 0.48 for dissociation from NH_3-$(\tilde{A}^1A_2'', v_2 = 6)$, but that no $ND_2(\tilde{A}^2A_1)$ was produced from the excitation of $ND_3(\tilde{A}^1A_2'', v_2 = 6)$.[13] Although we observed $ND_2(\tilde{A}^2A_1)$ in contrast to this earlier study, this qualitative trend for a lower yield of $ND_2(\tilde{A}^2A_1)$ than $NH_2(\tilde{A}^2A_1)$ from their respective parents supports the conclusion that the dissociation of ND_3 is more stringently confined to geometries close to planarity and, thus, dissociation to the ground electronic state fragments is preferred.

Examination of the vibrational excitation of the $ND_2(\tilde{A})$ fragment shows a greatly reduced degree of vibrational excitation in the ND_2 product from the dissociation of ND_3, compared to that of $NH_2(\tilde{A})$ from NH_3. As shown in Figure 1, from a purely classical argument the bending excitation of the product must predominantly result from dissociating geometries that are close to planar. If the dissociation of ND_3 leads to a tight confinement of the N−D bond to geometries near planarity as the molecule dissociates, those geometries close to planar that lead to vibrational excitation may be preferentially channeled down the conical intersection to ground electronic state products. In the dissociation of NH_3, a wider range of angular geometries is possible during the dissociation and this can give vibrational excitation in the electronically excited product fragment.

In support of this hypothesis, the ND_2 fragment produced in the photodissociation of ND_2H has a much higher level of vibrational excitation. The zero-point energy of the ground state of ND_2H is larger than that of ND_3 and, thus, the direct dissociations through planar geometries are less constrained in the angular coordinate as a higher energy in the excited electronic state parent is accessed. This permits the vibrational excitation in the excited-state fragment to arise following the sampling of a wide angular range during the dissociation, which may involve H atom tunneling. However, a conflicting factor that must also be considered is that nonadiabatic dissociations are expected to play a greater role in the cleavage of the N−H bond rather than the N−D bond. This suggests that the

nonadiabatic coupling to the ground electronic state fragments can occur at a larger range of out-of-plane angles for ND_2H than for ND_3. Thus, the increased yield of ND_2 from ND_2H in the excited state may reflect a much larger increase in the total quantum yield for dissociation to both the ground and electronically excited states.

A deficiency in this explanation is the extent of the minor-axis rotational excitation that occurs along with the vibrational excitation of the ND_2 fragment in the dissociation of ND_2H. We noted that the vibrationally excited bands of $ND_2(\tilde{A})$, which are spaced by the ground-state vibrational constant of ND_2, have a complicated structure associated with the $N' > K_a'$ excitation in the ND_2 ($\tilde{A}$, $v_2' = 1, 2$) product. This suggests that the vibrationally excited ND_2 product from the dissociation of ND_2H has a significantly different dissociation mechanism than that considered up to this point, which leads to a larger partitioning of rotational energy about the *b/c*-axes and, thus, the breakdown in the approximate treatment of the rotor as a symmetric-prolate top. One plausible explanation is that the vibrational mode of the parent ND_2H molecule that leads to dissociation may not be a pure umbrella bending mode. Although the $\tilde{A} \leftarrow \tilde{X}$ absorption spectrum of ND_2H appears to consist of a progression in the umbrella bending mode, analogous to that observed for the other parent species, it may be that a Fermi-resonance exists between the umbrella bending mode and another vibrational mode. To elucidate the character of the excited vibrational mode in the ND_2H parent would require both extensive computational work and the determination of the jet-cooled absorption spectrum of ND_2H, both of which are beyond the scope of the study presented here. However, based on the vibrational constants for ND_2H ($\tilde{A}$) measured by Lehmann and coworkers,[15,16] we excite the 2_0^7 transition of the $\tilde{A} \leftarrow \tilde{X}$ absorption spectrum, and this may lie very close to the 4_0^5 transition. In addition, reducing the symmetry of the parent molecule from C_{3v} to C_s by isotopic substitution will permit the ν_2 and ν_4 modes to mix. In ND_3, ν_2 has purely a_1 symmetry while ν_4 has e symmetry. However, in ND_2H, ν_2 has a' symmetry while ν_4 has $a' + a''$ symmetry. Coupling of the vibrational excitation of the parent molecule directly into the ν_4 scissors bending mode would be an extreme case of the effect observed of carry over of the zero-point motion of the ν_4 mode into *b/c*-axis rotational excitation. Exciting a vibrational mode with some ν_4 scissors bending mode character could lead directly to an extreme amount of *b/c*-axis product excitation in $ND_2(\tilde{A})$, as observed.

In contrast, the low degree of minor *b/c*-axes rotational excitation in $ND_2(\tilde{A}, v_2' = 0)$ suggests that the mechanism for N−H bond cleavage in this case is predominantly the same as that for producing NH_2 and ND_2 from NH_3 and ND_3, respectively. As illustrated in Figure 8, the high K_a states of $ND_2(\tilde{A}, v_2' = 0)$ from ND_2H have the same level of excitation as ND_2 from ND_3, within the signal-to-noise of the experiments presented here. The change in zero-point energy of the ν_4 vibrational mode between ND_3 (410 cm^{-1}) and ND_2H (510 cm^{-1})[11] is not sufficient to observe a change in the energy partitioning around the minor *b/c*-axes of the ND_2 fragment.

Only weak spectral signatures are observed from $NHD(\tilde{A})$ photofragments. This could possibly result from much smaller $\tilde{A} - \tilde{X}$ Einstein *A* coefficients for NHD than for NH_2 and ND_2; although the magnitudes of these for NHD are unknown. Alternatively, the low yield of $NHD(\tilde{A})$ from ND_2H dissociation can be rationalized if cleavage of the N−H bond dominates over cleavage of one of the two N−D bonds. Also, and perhaps most important is that the N−H bond is weaker than the N−D bond.[11] The enhanced yield in the product ND_2 ($\tilde{A}$, $v_2' = 0$) from ND_2H over that from ND_3 has already been noted and has been attributed to the greater tunneling efficiency of H atoms over D atoms. Thus, the dominance of N−H over N−D bond cleavage in the adiabatic dissociation of ND_2H is very likely an important conclusion. This, however, does not explain the apparently small yield of NHD on the excited electronic state from the photodissociation of NH_2D. Based on the discussion above, NHD should be the dominant product in this case, and, indeed, $NHD(\tilde{X})$ has been observed as the primary channel in the nonadiabatic dissociation to the ground-state fragment from this parent species.[11] Mordaunt et al. have also noted that a significant proportion of the electronically excited NH_2D parent undergoes internal conversion to high lying dissociative states of the ground electronic state, and this may also result in a much lower yield of the adiabatic photodissociation products of NH_2D.[11] It should be reiterated that the absorption cross-section of NH_2D at room-temperature is considerably lower than those of the other parent species. Further, very little $NH_2(\tilde{A}, v_2' = 0, 1, 2)$ is observed as a photoproduct from NH_2D. This suggests that the signal-to-noise ratio of the experiments presented here is simply not sufficient to probe the fragments from the photodissociation of NH_2D.

VII. Summary

We have undertaken a comprehensive study of the adiabatic photodissociation dynamics of all four of the isotopomers of ammonia, NH_3, NH_2D, ND_2H, and ND_3.[2,3] Techniques have been developed to extract the product state information from complex product emission spectra,[20] which contain spectral signatures from the photodissociation dynamics of six competing photofragmentation pathways, and this has this led to a refined understanding of the mechanism of the N−H(D) bond cleavage.

In all cases, bimodal rotational distributions about the primary *a*-axis have been observed, and we attribute this energy partitioning to the competition between two mechanisms for bond cleavage that may sample very different regions of the potential energy surface as the dissociating bond lengthens. Dissociations through out-of-plane geometries lead to high rotational excitation about the *a*-axis, while planar geometries lead to low rotational excitation. We have also suggested that the competition between tunneling dissociations from large out-of-plane angles and direct dissociation at planar geometries may be important. Not only does this influence the rotational energy partitioning in the product fragments, but it also may influence the competition between adiabatic and nonadiabatic dynamics, with adiabatic dissociations preferentially occurring at large out-of-plane bending angles. We have shown that ND_2H preferentially dissociates to the excited ND_2 fragment with cleavage of the N−H bond, while NH_2D shows a comparatively lower probability for dissociation to the excited electronic state fragments NH_2 or NHD compared with NH_3, ND_2H, and ND_3.

The energy partitioning about the minor *b/c*-axes has been shown to result from the zero-point bending motion in the υ_4 scissors bending vibration of the parent molecule. While this is in qualitative agreement with theoretical models, it is essential that further models that study the adiabatic dissociation dynamics of ammonia be undertaken before the legitimacy of our other hypotheses can be tested.

Acknowledgment. The authors thank the Department of Energy for support of this research and the National Science Foundation for additional equipment. R.A.L. gratefully acknowledges the support of the National Research Council for a Postdoctoral Fellowship with the National Institute of Standards

and Technology. The authors also thank Professor Charles Qian for invaluable discussions.

References and Notes

(1) Schinke, R. *Photodissociation Dynamics*; University Press: Cambridge, Great Britain, 1993.
(2) Loomis, R. A.; Reid, J. P.; Leone, S. R. *J. Chem. Phys.* **2000**, *112*, 658.
(3) Reid, J. P.; Loomis, R. A.; Leone, S. R. *Chem. Phys. Lett.* **2000**, in press.
(4) Leone, S. R. *Acc. Chem. Res.* **1989**, *22*, 139.
(5) Rogers, S. A.; Leone, S. R. *Appl. Spectrosc.* **1993**, *47*, 1430.
(6) Hancock, G.; Heard, D. E. In *Advances in Photochemistry*; Volman, D. H., Hammond, G. S., Neckers, D. C., Eds.; Wiley: New York, 1993; Vol. 18, p 1.
(7) Sloan, J. J. *Advances in Spectroscopy*; Wiley: New York, 1989.
(8) McCarthy, M. I.; Rosmus, P.; Werner, H.-J.; Botschwina, P.; Vaida, V. *J. Chem. Phys.* **1987**, *86*, 6693.
(9) Rosmus, P.; Botschwina, P.; Werner, H.-J.; Vaida, V.; Engelking, P. C.; McCarthy, M. I. *J. Chem. Phys.* **1987**, *86*, 6677.
(10) Vaida, V.; McCarthy, M. I.; Engelking, P. C.; Rosmus, P.; Werner, H.-J.; Botschwina, P. *J. Chem. Phys.* **1987**, *86*, 6669.
(11) Mordaunt, D. H.; Dixon, R. N.; Ashfold, M. N. R. *J. Chem. Phys.* **1996**, *104*, 6472.
(12) Biesner, J.; Schnieder, L.; Schmeer, J.; Ahlers, G.; Xie, X.; Welge, K. H.; Ashfold, M. N. R.; Dixon, R. N. *J. Chem. Phys.* **1988**, *88*, 3607.
(13) Biesner, J.; Schnieder, L.; Ahlers, G.; Xie, X.; Welge, K. H.; Ashfold, M. N. R.; Dixon, R. N. *J. Chem. Phys.* **1989**, *91*, 2901.
(14) Woodbridge, E. L.; Ashfold, M. N. R.; Leone, S. R. *J. Chem. Phys.* 1**991**, *94*, 4195.
(15) Henck, S. A.; Mason, M. A.; Yan, W.-B.; Lehmann, K. K.; Coy, S. L. *J. Chem. Phys.* **1995**, *102*, 4772.
(16) Henck, S. A.; Mason, M. A.; Yan, W.-B.; Lehmann, K. K.; Coy, S. L. *J. Chem. Phys.* **1995**, *102*, 4783.
(17) Mordaunt, D. H.; Ashfold, M. N. R.; Dixon, R. N. *J. Chem. Phys.* **1996**, *104*, 6460.
(18) Mordaunt, D. H.; Ashfold, M. N. R.; Dixon, R. N *J. Chem. Phys.* **1998**, *109*, 7659.
(19) Dixon, R. N. *Mol. Phys.* **1996**, *88*, 949.
(20) Reid, J. P.; Loomis, R. A.; Leone, S. R. *J. Chem. Phys.* **2000**, *112*, 3181.
(21) Jacobson, M. P.; Coy, S. L.; Field, R. W. *J. Chem. Phys.* **1997**, *107*, 8349.
(22) Coy, S. L.; Jacobson, M. P.; Field, R. W. *J. Chem. Phys.* **1997**, *107*, 8357.
(23) Douglas, A. E. *Faraday Discuss. Chem. Soc.* **1963**, *35*, 158.
(24) Vaida, F.; Hess, W. E.; Roebber, J. L. *J. Chem. Phys.* **1984**, *88*, 3397.
(25) Suto, M.; Lee, L. C. *J. Chem. Phys.* **1983**, *78*, 4515.
(26) Proch D.; Trickl, T. *Rev. Sci. Instrm.* **1989**, *60*, 713.
(27) Seelemann, T.; Andresen, P.; Schleipen, J.; Beyer, B.; Ter Meulen, J. J. *Chem. Phys.* **1988**, *126*, 27.
(28) Ebel, G.; Krohne, R.; Meyer, H.; Buck, U.; Schinke, R.; Seelemann, T.; Andresen, P.; Schleipen, J.; ter Meulen, J. J.; Diercksen, G. H. F. *J. Chem. Phys.* **1990**, *93*, 6419.
(29) Dressler, K.; Ramsay, D. A. *Philos. Trans. R. Soc. A* **1959**, *251*, 553.
(30) Ross, S. C.; Birss, F. W.; Vervloet, M.; Ramsay, D. A. *J. Mol. Spec.* **1988**, *129*, 436.
(31) Bolvin, H.; Demuynck, C.; Destombes, J.-L.; Bachir, I. H.; Huet, T. R.; Cireasa, R.; Vervloet, M. *Astron. Soc. Pac. Conf. Ser. (Laboratory and Astronomical High-Resolution Spectra)* **1995**, *81*, 282.
(32) Jungen, C.; Hallin, K.-E. J.; Merer, A. J. *Mol. Phys.* **1980**, *40*, 25.
(33) Jungen, C.; Hallin, K.-E. J.; Merer, A. J. *Mol. Phys.* **1980**, *40*, 65.
(34) Duxbury, G.; Dixon, R. N. *Mol. Phys.* **1981**, *43*, 255.
(35) Herzberg, G. *Molecular Spectra and Molecular Structure III. Electronic Spectra and Electronic Structure of Polyatomic Molecules*; Van Nostrand-Reinhold: New York, 1966.
(36) Duxbury, G., private communication, 1998.
(37) Bevington, P. R. *Data Reduction and Error Analysis for the Physical Sciences*; McGraw-Hill: New York, 1969.